AD-A141 378 DYNAMIC BEHAVIOR OF PULSED IMPATT OSCILLATORS(U) 1/1
MICHIGAN UNIV ANN ARBOR DEPT OF ELECTRICAL AND COMPUTER
ENGINEERING R K MAINS ET AL. 1981 N60530-81-C-0364
UNCLASSIFIED F/G 9/5 NL

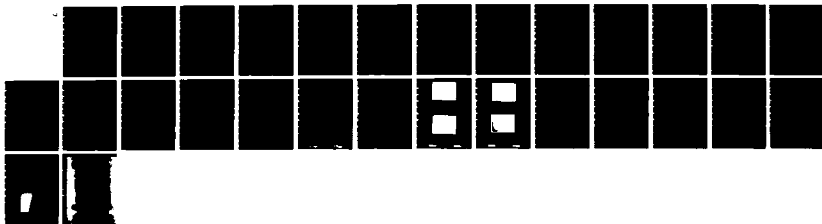

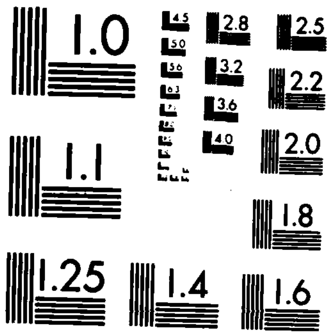

MICROCOPY RESOLUTION TEST CHART
NATIONAL BUREAU OF STANDARDS-1963-A

AD-A141 378

DYNAMIC BEHAVIOR OF PULSED IMPATT OSCILLATORS*

R. K. Mains and G. I. Haddad

Electron Physics Laboratory
Department of Electrical and Computer Engineering
The University of Michigan
Ann Arbor, MI 48109

D. Bowling and M. Afendykiw

Naval Weapons Center
China Lake, CA 93555

N60530-81-C-0364

ABSTRACT

A method of simulating the dynamic behavior of pulsed IMPATT oscillators is presented. It is assumed that the simulation variables change slowly with respect to the RF period so that the quasi-static approximation may be used. A comparison of simulation results with experimental results for an X-band circuit is given.

MAY 2 1984

A

This document has been approved for public release and sale; its distribution is unlimited.

DTIC FILE COPY

*This work was supported by the Naval Weapons Center, China Lake, CA.

84 05 21 128

INTRODUCTION

The quasi-static approximation may be effectively used to simulate transient effects in free-running and injection-locked pulsed oscillators [1],[2]. It is an alternative to the time-consuming method of performing a complete device-circuit interaction simulation in the time domain using a small time step due to stability restrictions on the device simulation. The quasi-static method requires a complete steady-state characterization of the IMPATT device over the ranges of temperature, bias current density and RF voltage amplitude that will be encountered in the transient simulation. It is then assumed that the simulation parameters change slowly with respect to the RF period so that the IMPATT appears to be in a steady-state condition at any particular instant of time. In this manner the transient can readily be simulated over the entire pulse width.

IMPATT DEVICE MODEL

Figure 1 shows the doping profile of the GaAs double-drift IMPATT diode used in the simulations. This particular structure was fabricated by Microwave Associates, Inc., and was also used in the experimental phase of the investigation. This diode was simulated at 10 GHz using the computer programs developed by Bauhahn and Haddad [3],[4] and later modified by Mains and Haddad [5], wherein it is assumed that the particle currents consist of a drift plus diffusion term, with drift velocities and diffusion coefficients expressed as functions of the local electric field. Simulations

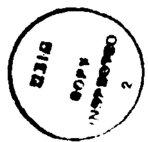

Codes
and/or
Dist | Special
A-1

were carried out at temperatures T = 300, 400, 500, 535 and 575°K. At each temperature, simulations were performed at bias current densities of J_{dc} = 400, 650 and 1000 A/cm^2. For each (T, J_{dc}) combination, a sinusoidal RF voltage at 10 GHz was applied and the amplitude was varied from zero to the point where the diode efficiency dropped significantly. The information thus obtained is $Y_D(f = 10$ GHz; $T, J_{dc}, V_{RF})$, the diode admittance in mho/cm^2, and V_{dc} $(f = 10$ GHz; $T, J_{dc}, V_{RF})$, the diode large-signal operating voltage. At $J_{dc} = 0$, the diode is modeled as a depletion capacitance, $C_o = (\varepsilon A/w_d)$F, in series with a small resistor, $R_o = (w_u/\sigma A)\Omega$, to account for the undepleted region (w_d is the depletion region width and w_u is the width of the undepleted region). To obtain the diode characteristics at operating points other than those simulated, a linear interpolation scheme is used [2].

It is assumed that the circuit admittance $Y_c(s)$ varies more rapidly with frequency than the diode admittance so that Y_D may be assumed constant with frequency over the frequency range of interest. However, the diode cold capacitance $C_D = (\varepsilon/w)$ F/cm^2 (where $w = w_d + w_u$ = 6.95 μm) is lumped into $Y_c(s)$ so that the ωC_D component of the diode susceptance does vary with frequency. The device area was assumed to be $A = 1.3 \times 10^{-3}$ cm^2 which is the measured value for the diode.

CIRCUIT MODEL

Figure 2 shows the circuit used to model the actual oscillator circuit, which consists of a 50-Ω transmission line (represented by R_L) and a low-impedance transformer adjacent to the diode package (represented by Z_c, ℓ, and ε_r). The capacitance C is the discontinuity capacitance between the 50-Ω transmission line and the

transformer. The circuit elements to the right of plane I were verified from experimental impedance measurements at this plane. It was attempted to measure the package-mounting equivalent circuit elements L_s and C_p however some uncertainty remained concerning these values, especially for the series inductance L_s. The procedure was to use the experimentally determined value of 0.32 pF for C_p and to determine L_s as follows. The diode admittance resulting from the simulation at T = 500°K, J_{dc} = 650 A/cm^2 (the bias current density used experimentally) and V_{RF} = 57.17 V [maximum efficiency point for this particular (T, J_{dc}) combination] was transformed through the package-mounting equivalent circuit to plane I in Fig. 2. L_s was then chosen so that this transformed admittance was equal to the experimental large-signal admittance measurements at plane I. C_D is the diode cold capacitance, which is lumped into the circuit model.

QUASI-STATIC, DEVICE-CIRCUIT INTERACTION SIMULATION PROCEDURE

Figure 3 indicates the overall procedure used in the simulation. In Fig. 3(a), $Y_c(s)$ is the admittance vs. complex frequency s of the circuit in Fig. 2 at plane I, $Y_D(V_{RF}, J_{dc}, T)$ is the diode admittance determined from the large-signal device simulation, $I_i(\omega_c)$ is the injection current used to simulate the injection-locked case. V_{RF} is the (peak) amplitude of the RF voltage at the diode terminals, and ϕ is the phase of this voltage relative to $I_i(\omega_c)$. Both V_{RF} and ϕ are slowly varying functions of time. The complex frequency s is obtained at each time step by solving the equation:

$$Y_c(s) + Y_D(V_{RF}, J_{dc}, T) = \frac{I_\ell}{V_{RF}} e^{-j\phi} \quad . \qquad (1)$$

V_{RF} and ϕ are updated according to

$$\frac{1}{V_{RF}} \frac{dV_{RF}}{dt} = \sigma = Re\{s\} \qquad (2)$$

and

$$\frac{d\phi}{dt} = \omega - \omega_o = Im\{s\} - \omega_o \quad . \qquad (3)$$

The diode temperature T is updated from

$$\frac{dT}{dt} = \frac{R_{th} P_D}{\tau} - \frac{T - T_A}{\tau} \quad , \qquad (4)$$

where R_{th} is the diode thermal resistance in $^{o}K/W$, P_D is the power dissipated in the diode in W, T_A is the ambient temperature in ^{o}K, and τ is the thermal relaxation time in seconds.

In Fig. 3(b), the bias current J_{dc} is assumed to rise linearly from zero to a constant value at turn on, to maintain this constant value throughout the pulse width, and then to fall linearly to zero at turn off. In principle, the bias circuit could be modeled and a second device-circuit interaction could be solved to determine the evolution of J_{dc} with time, however, this was not done in the simulations presented here.

For the injection-locked case, it is assumed that I_ℓ is on long before the bias current density J_{dc} is switched on at t = 0. Therefore, at t = 0 a substantial RF voltage exists across the diode terminals even though the device is passive at this time.

COMPARISON OF THEORETICAL AND EXPERIMENTAL RESULTS

Figure 4 presents the turn-on and turn-off characteristics observed for the free-running case and Fig. 5(a) shows the behavior over the entire 1.5-μs pulse. The diode was found to oscillate at 9.7 GHz, the peak output power was 15.8 W, and the diode operating voltage was approximately 100 V. Figure 5(b) shows that, for the injection-locked case, the diode turns on faster than for the free-running case. (In Figs. 4 and 5, an additional 6 ns delay is introduced in the detected RF waveform relative to the bias current waveform due to the measurement setup.)

Table 1 shows the experimental results for the injection-locked case as the injection signal power is varied. The injection frequency was 10 GHz and the (peak) bias current was $I_b = 0.84$ A, or $J_{dc} = 646$ A/cm^2. P_{RF} is the (peak) RF power generated by the IMPATT and does not include the power delivered by the injection source P_{in}. T_j is the average junction temperature calculated from the experimentally determined thermal resistance. It was found experimentally that if the injection power was reduced below 2 W, the IMPATT did not lock with the injection source.

The thermal resistance was experimentally determined to be $R_{th} = 5°K/W$ for the diode and 1°K/W for the mount. Since the temperature in the mount changes more slowly than the diode temperature [6], the 1°K/W contribution was assumed to increase the ambient temperature, T_A in (4), from room temperature as follows:

$$T_A = 300°K + 64.7\ W \times 0.45 \times 1°K/W = 329°K \quad , \qquad (5)$$

where 64.7 W is the peak dissipated power in the diode and 0.45 is the

duty factor. The IMPATT diodes were fabricated in a quad mesa structure; an appropriate thermal relaxation time for this arrangement is $\tau = 8\ \mu s$ in (4). Using these values, (4) implies that, in order for the average diode temperature to be 473°K (see Table 1), the diode temperature at the beginning of the bias current pulse must be approximately 460°K in the steady state.

Figure 6(a) shows the start-up behavior obtained from the quasi-static simulation for the free-running case. For comparison, the corresponding portion of the experimentally observed RF power from Fig. 4(a) is also shown. The amplitude of the experimental curve is normalized so that both the experimental and theoretical curves reach the same maximum RF power level. The bias current increases linearly from zero at $t = 0$ to $J_{dc} = 646\ A/cm^2$ at $t = 60$ ns in Fig. 6(a). The starting temperature at $t = 0$ is 460°K. From Fig. 4(a), the detected RF power turns on approximately 32 ns after the bias current begins to increase (recall the additional 6-ns delay in the measurement system); this experimental delay is very close to the delay resulting from the simulation in Fig. 6(a). Figure 6(b) shows a plot of the circuit admittance vs. real frequency ($\sigma = 0$) and small-signal device admittance vs. J_{dc} at the starting temperature $T = 460$°K. From (2), V_{RF} will not increase until (1) is satisfied for a value of s such that $Re\{s\} = \sigma > 0$. In Fig. 6(b), the region to the right of the $- Y_c(f)$ curve corresponds to $- Y_c(s)$ values such that $Re\{s\} < 0$, and the area to the left of the $-Y_c(f)$ curve contains $- Y_c(s)$ values such that $Re\{s\} > 0$. As J_{dc} increases from zero to 200 A/cm^2, the Y_L and $- Y_c(s)$ curves cross for $\sigma < 0$ values and V_{RF} cannot increase. As J_{dc} increases further, the Y_L curve enters the $\sigma > 0$ region and V_{RF} begins to build up. From Fig. 6(b), it is seen that the oscillation

frequency will start at approximately 9.7 GHz, which is the experimentally observed frequency for the free-running case.

Figure 7 shows the RF power simulated during the oscillator turnoff where it is assumed that J_{dc} decreases linearly from 646 A/cm^2 at $t = 0$ to zero at $t = 90$ ns. This result should be compared with Fig. 4(b), although in the experiment J_{dc} departs from the linear waveform.

Figure 8 shows the start-up transient for the injection-locked case, with $I_\ell = 0.557$ A [see (1) and Fig. 3(a)] so that the incident power from the locking source is $I_\ell^2/8G_c = 4$ W at 10 GHz. Comparison of Fig. 8 with Fig. 6(a) shows that the RF power turns on faster for the injection-locked case than for the free-running case. This is in agreement with the experimental result shown in Fig. 5(b). This is because there is a substantial RF voltage across the diode at $t = 0$ due to the injection source.

Table 2 presents the simulation results as the injection power is varied from 2.0 to 6.0 W. Comparison with Table 1 shows that the same general RF power variation as observed experimentally is predicted by the simulation, although the simulation predicts a power maximum at $P_{in} = 4.0$ W instead of 3.5 W, and the maximum power predicted by the simulation is 16.56 W instead of 17.63 W.

The behavior indicated in Table 2 can be understood by examining the curves in Fig. 9. Since, for injection-locking, (1) must be satisfied, the magnitude of the injection current source I_L must satisfy the following relation at the start of the pulse (after the bias current has reached its maximum value):

$$I_L = V_{RF}|Y_c(f=10 \text{ GHz}) + Y_D(T=460°K, J_{dc}=646 \text{ A/cm}^2; V_{RF})| \quad . \quad (6)$$

V_{RF} (the magnitude of the RF voltage at the diode terminals) and the corresponding $Y_D(V_{RF})$ were previously obtained by the diode characterization process, using the steady-state IMPATT simulation program. Equation (6) matches each V_{RF} value with a corresponding I_L for steady-state locking. Also, for each V_{RF} the RF power generated by the diode is

$$P_{RF} = -\frac{1}{2} G_D V_{RF}^2 \quad , \tag{7}$$

where $G_D = Re\{Y_D(V_{RF})\}$. The expressions in (6) and (7) are plotted in Fig. 9. It is seen that as I_L is varied from 300 A/cm^2 (0.39 A) to 800 A/cm^2 (1.04 A), the RF power first increases, reaches a maximum for I_L = 450 A/cm^2 (0.585 A), and then decreases. (P_{RF} in Fig. 9 is the RF power at the start of the pulse, whereas the RF power in Table 2 is the average over the 1.5-μs pulse width). Below $I_L \cong$ 285 A/cm^2 (0.370 A, P_{in} = 1.76 W), it is anticipated from Fig. 9 that locking cannot occur except perhaps at very low P_{RF} values. (It must also be investigated whether the operating points in Fig. 9 are stable.) This expectation is borne out by the simulation in Fig. 10 for which P_{in} = 1.5 W (I_L = 0.341 A). The diode does not lock until it has heated up to 477°K, so that the curves in Fig. 9 are no longer applicable. As the diode continues to heat up the generated RF power gradually increases to 14.9 W. This behavior is consistent with the experimental results, since for P_{in} much below 2 W the locking at 10 GHz was not found to be stable.

CONCLUSIONS

It has been shown that a large-signal IMPATT diode simulation program employing the drift-diffusion approximation in conjunction

with a quasi-static transient simulation can accurately predict experimentally observed behavior at 10 GHz, both for the free-running and injection-locked cases. These programs may be used for diode and circuit design at higher frequencies where measurements become more difficult. However, it may be necessary to include relaxation effects in the IMPATT diode simulation since it has been shown that these effects become significant at low millimeter-wave frequencies [7].

LIST OF REFERENCES

1. H. Kurokawa, "Injection locking of microwave solid-state oscillators," Proc. IEEE, vol. 61, pp. 1386-1410, Oct. 1973.

2. R. K. Mains, G. I. Haddad and D. F. Peterson, "Simulation of pulsed IMPATT oscillators and injection-locked amplifiers," Tech. Report No. AFWAL-TR-81-1177, Electron Physics Laboratory, The University of Michigan, Ann Arbor, Feb. 1981.

3. P. E. Bauhahn and G. I. Haddad, "IMPATT device simulation and properties," IEEE Trans. Electron Devices, vol. ED-24, pp. 634-642, June 1977.

4. P. E. Bauhahn, "Properties of semiconductor materials and microwave transit-time devices," Ph.D. Dissertation, The University of Michigan, Ann Arbor, Oct. 1977.

5. R. K. Mains and G. I. Haddad, "Properties of high-efficiency X-band GaAs IMPATT diodes," Tech. Report No. AFWAL-TR-81-1066, Electron Physics Laboratory, The University of Michigan, Ann Arbor, June 1981.

6. L. H. Holway, Jr., "Transient temperature behavior in pulsed double-drift IMPATT diodes," IEEE Trans. Electron Devices, vol. ED-27, pp. 433-442, Feb. 1980.

7. R. K. Mains and G. I. Haddad, "Simulation of GaAs IMPATT diodes including energy and velocity transport equations," 1983 WOCSEMMAD Conf., San Antonio, TX, February 1983.

LIST OF FIGURES

Fig. 1 Doping profile of GaAs IMPATT diode used in the theoretical and experimental investigations (diode area $A = 1.3 \times 10^{-3}$ cm^2).

Fig. 2 Circuit model used for the simulations ($C_D = 2.07$ pF, $L_s = 0.253$ nH, $C_p = 0.32$ pF, $Z_c = 3.98\ \Omega$, $\varepsilon_r = 2.53$, $\ell = 0.2667$ cm, $C = 0.111$ pF and $R_L = 50\ \Omega$).

Fig. 3 (a) RF circuit and (b) bias circuit used in the simulation.

Fig. 4 Experimentally observed (a) turn-on and (b) turn-off behavior for the free-running case ($J_{dc} = 646$ A/cm^2, pulse width = 1.5 μs and duty cycle = 45%).

Fig. 5 (a) Bias current and RF power for the free-running case and (b) comparison between free-running and injection-locked turn-on characteristics (f_o = injection frequency = 10 GHz).

Fig. 6 (a) Start-up behavior for the free-running simulation [$J_{dc}(t = 0) = 0$, $J_{dc}(t = 60$ ns$) = 646$ A/cm^2 $T(0) = 460^\circ$K and $\tau = 8$ μs] and (b) admittance plot of $Y_D(V_{RF} = 0, T = 460^\circ\mathrm{K}; J_{dc})$ and $-Y_c(f)$.

Fig. 7 Turn-off characteristic for the free-running case [$J_{dc}(t = 0) = 646$ A/cm^2, $J_{dc}(t = 90$ ns$) = 0$ and $\tau = 8$ μs].

Fig. 8 RF power for the injection-locked start-up transient [$J_{dc}(t = 0) = 0$, $J_{dc}(t = 60$ ns$) = 646$ A/cm^2, $\tau = 8$ μs, $I_L = 0.557$ A, $P_{in} = 4.0$ W and $f_c = 10$ GHz].

Fig. 9 Locking-signal amplitude and generated RF power vs V_{RF} according to (6) and (7) ($f_o = 10$ GHz, $J_{dc} = 646$ A/cm^2, $A = 1.3 \times 10^{-3}$ cm^2 and $T = 460^\circ$K).

Fig. 10 RF power for the injection-locked case (J_{dc} = 646 A/cm^2, τ = 5 μs, I_L = 0.341 A, P_{in} = 1.5 W and f_c = 10 GHz).

LIST OF TABLES

Table 1 Injection-locked results observed experimentally as a function of injected power (f_o = 10 GHz, J_{dc} = 646 A/cm^2, pulse width = 1.5 μs and duty factor = 45%).

Table 2 Results of the quasi-static simulation for the injection-locked case. (J_{dc} = 646 A/cm^2, τ = 8 μs, f_o = 10 GHz, pulse width = 1.5 μs and duty factor = 45%. P_{RF} is averaged over the pulse width.)

Table 1

Injection-locked results observed experimentally

as a function of injected power

(f_o = 10 GHz, J_{dc} = 646 A/cm^2, pulse width = 1.5 μs and duty factor = 45%)

P_{in} (W, peak)	P_{RF} Added (W, peak)	Average T_J (°K)	Efficiency (%)	V_{dc} (V)
2.00	14.77	479.2	17.9	98.0
2.50	16.28	472.8	20.0	97.0
3.00	17.44	472.0	21.2	98.0
3.50	17.63	471.4	21.4	98.0
3.75	17.39	472.1	21.1	98.0
4.00	16.51	474.5	20.1	98.0
4.50	16.12	475.6	19.6	98.0
5.00	15.88	476.2	19.3	98.0

Table 2

Results of the quasi-static simulation for the injection-locked case (J_{dc} = 646 A/cm^2, τ = 8 μs, f_c = 10 GHz, pulse width = 1.5 μs and duty factor = [illegible]5%. P_{RF} is averaged over the pulse width.)

I_L (A)	P_{in} (W)	P_{RF} (W, peak)
0.394	2.0	15.50
0.4406	2.5	16.30
0.483	3.0	16.41
0.521	3.5	16.53
0.557	4.0	16.56
0.591	4.5	16.34
0.623	5.0	16.11
0.653	5.5	15.87
0.683	6.0	15.56

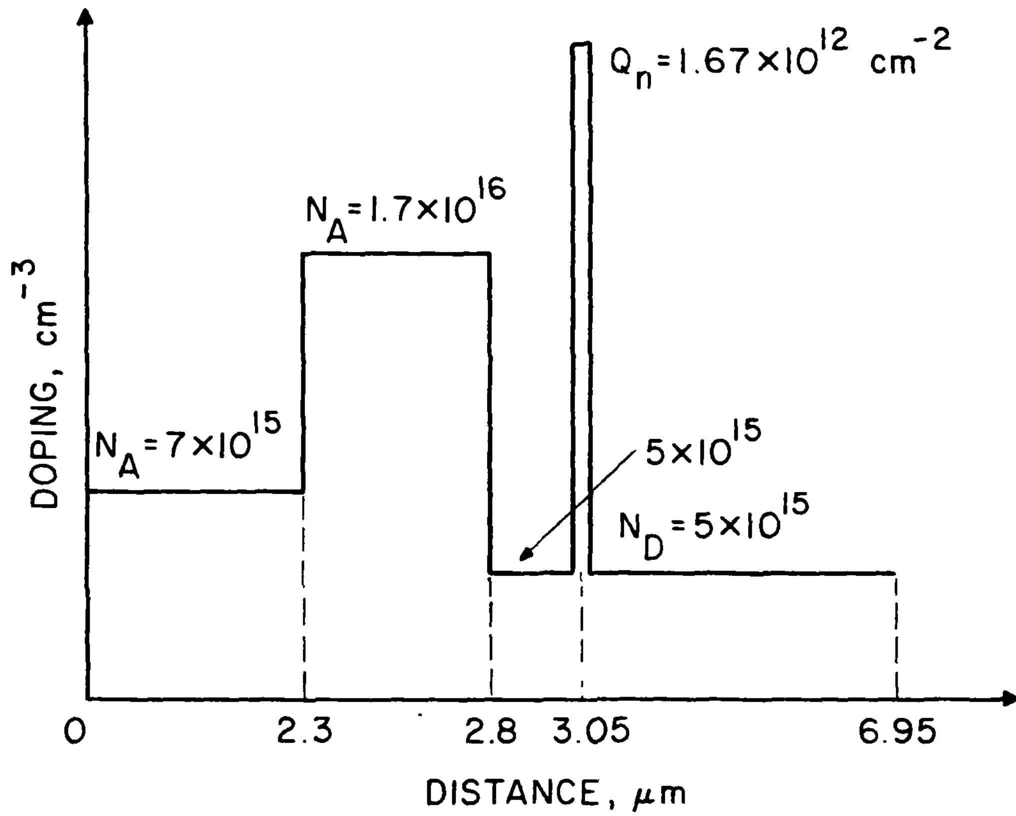

DOPING, cm^{-3}
$Q_n = 1.67 \times 10^{12}\ cm^{-2}$
$N_A = 1.7 \times 10^{16}$
$N_A = 7 \times 10^{15}$
5×10^{15}
$N_D = 5 \times 10^{15}$
0
2.3
2.8
3.05
6.95
DISTANCE, μm

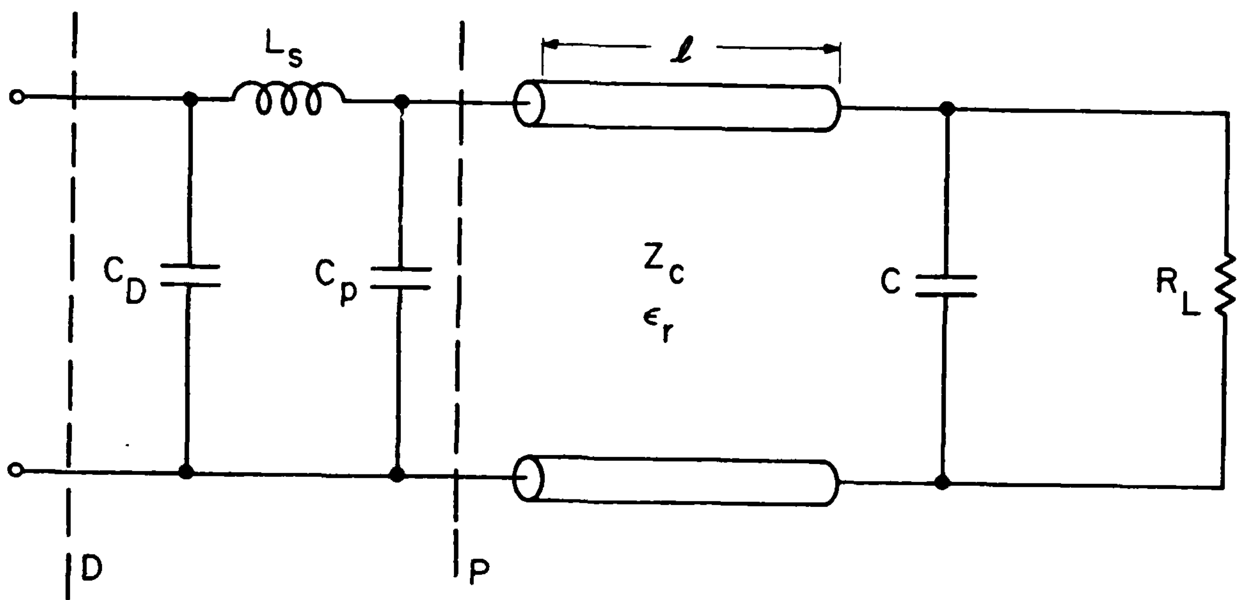

Ls
ℓ
CD
Cp
Zc
εr
C
RL
D
P

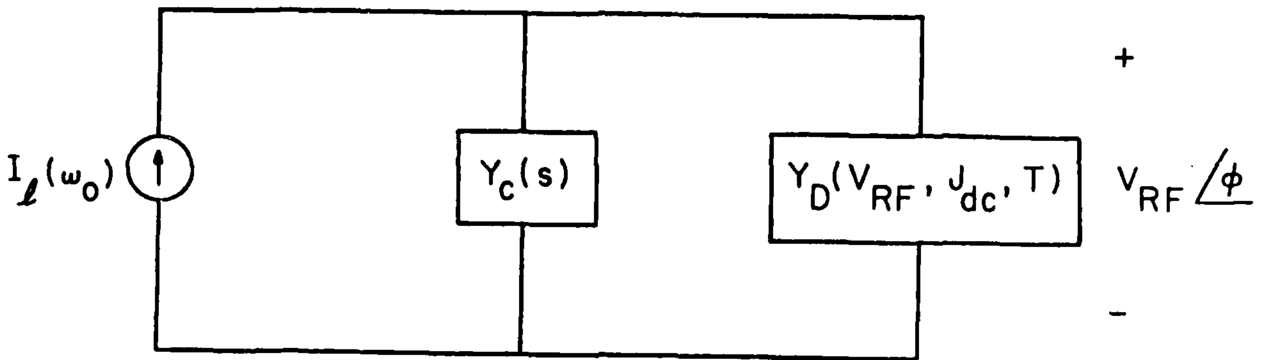

(a)

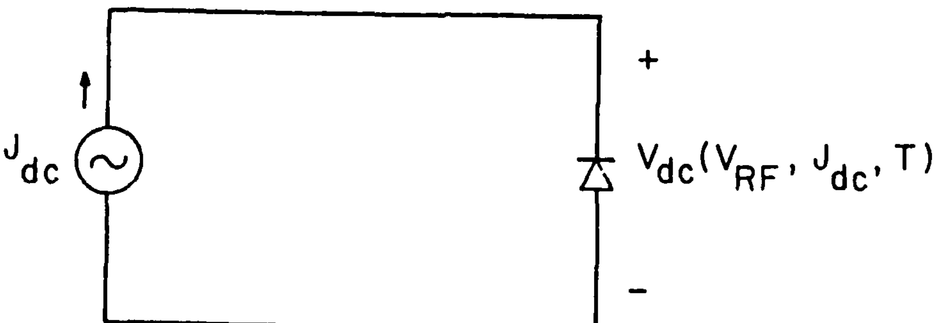

(b)

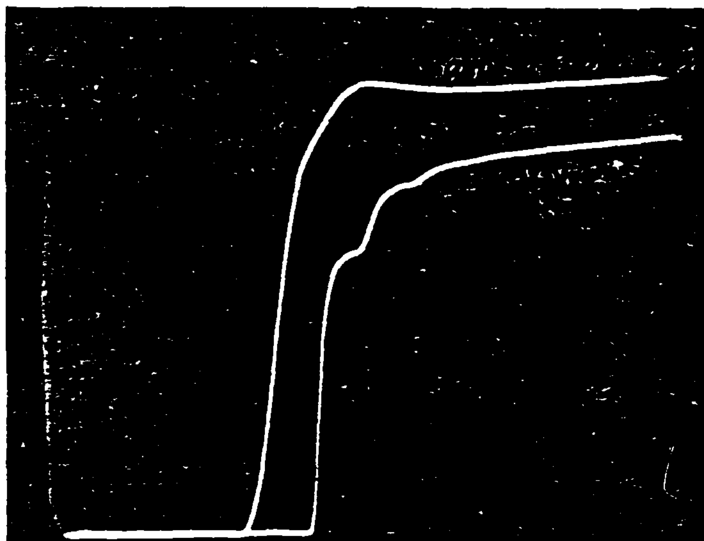

(a)

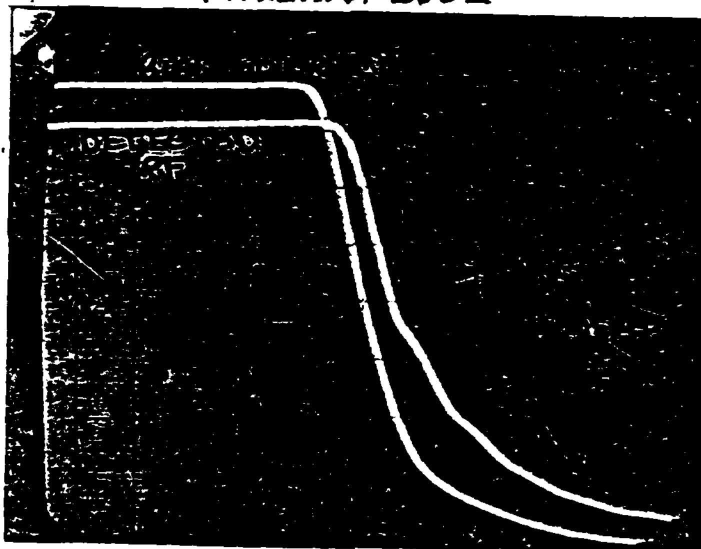

(b)

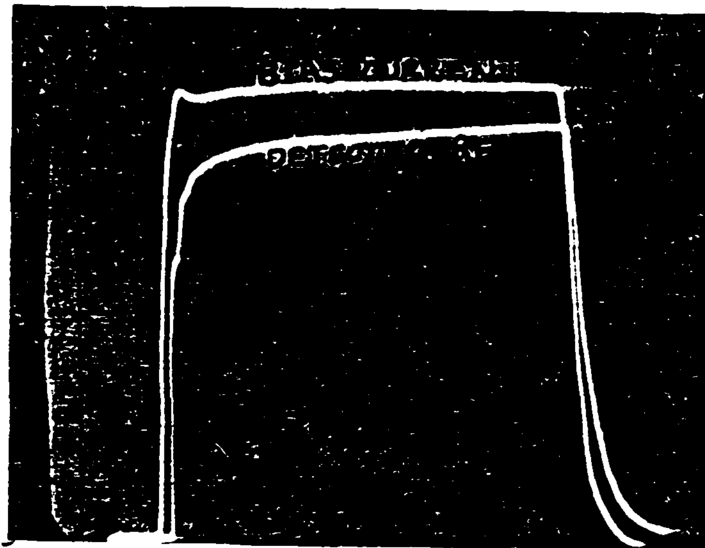

(a)

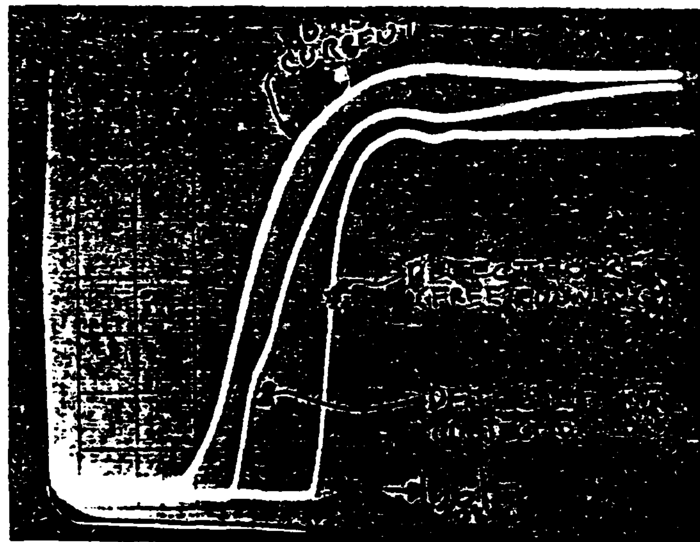

(b)

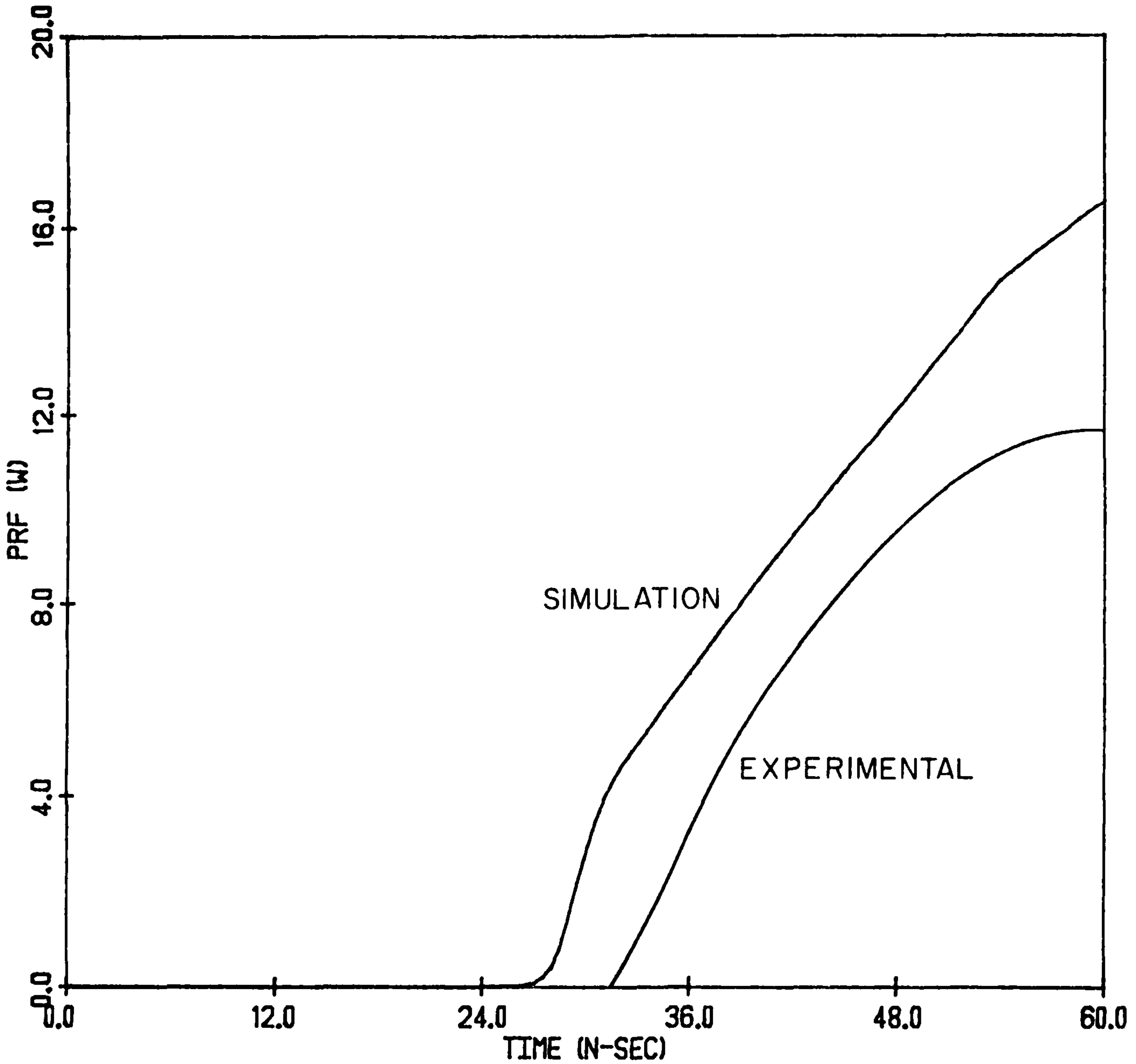

(a)

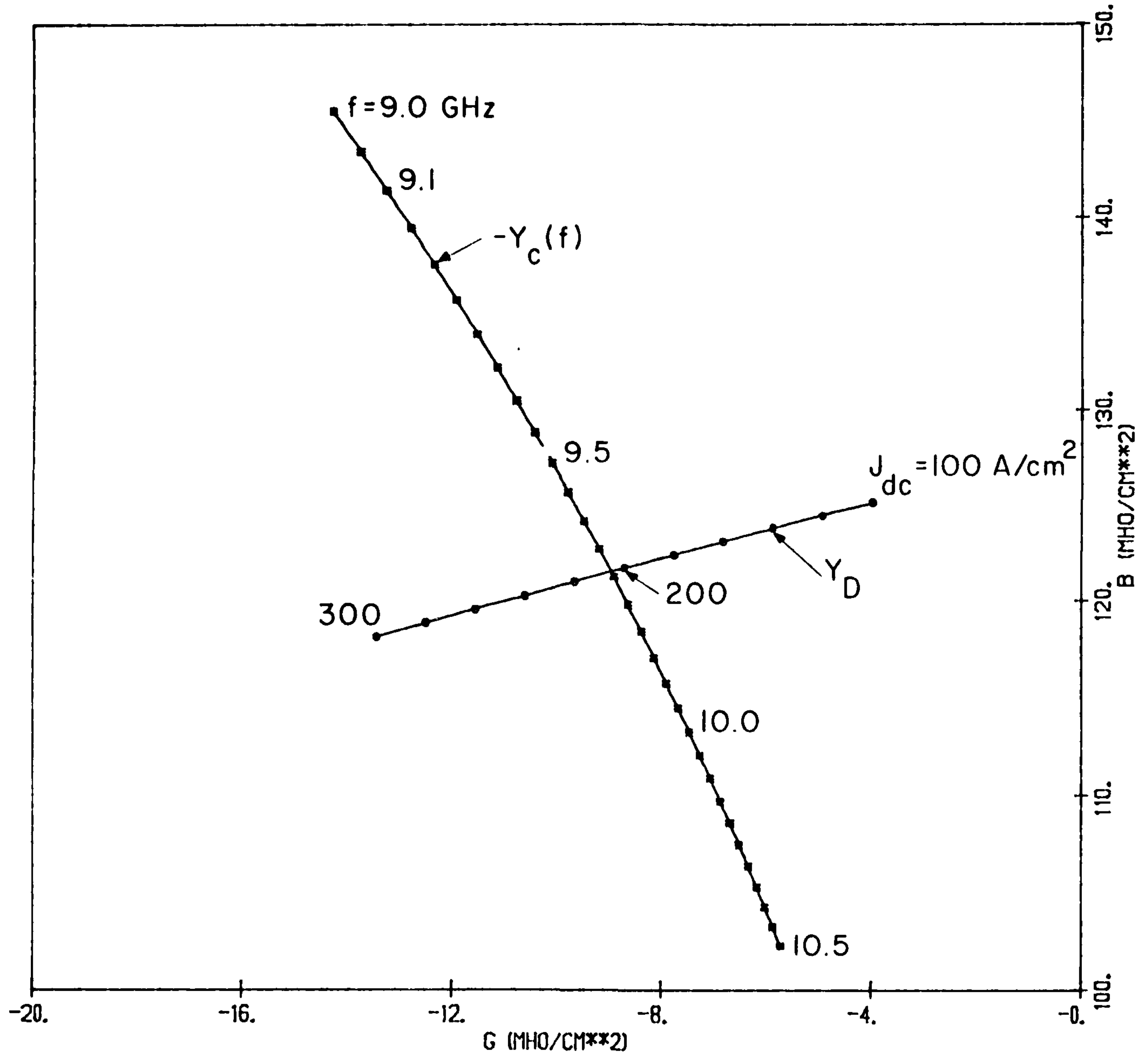

(b)

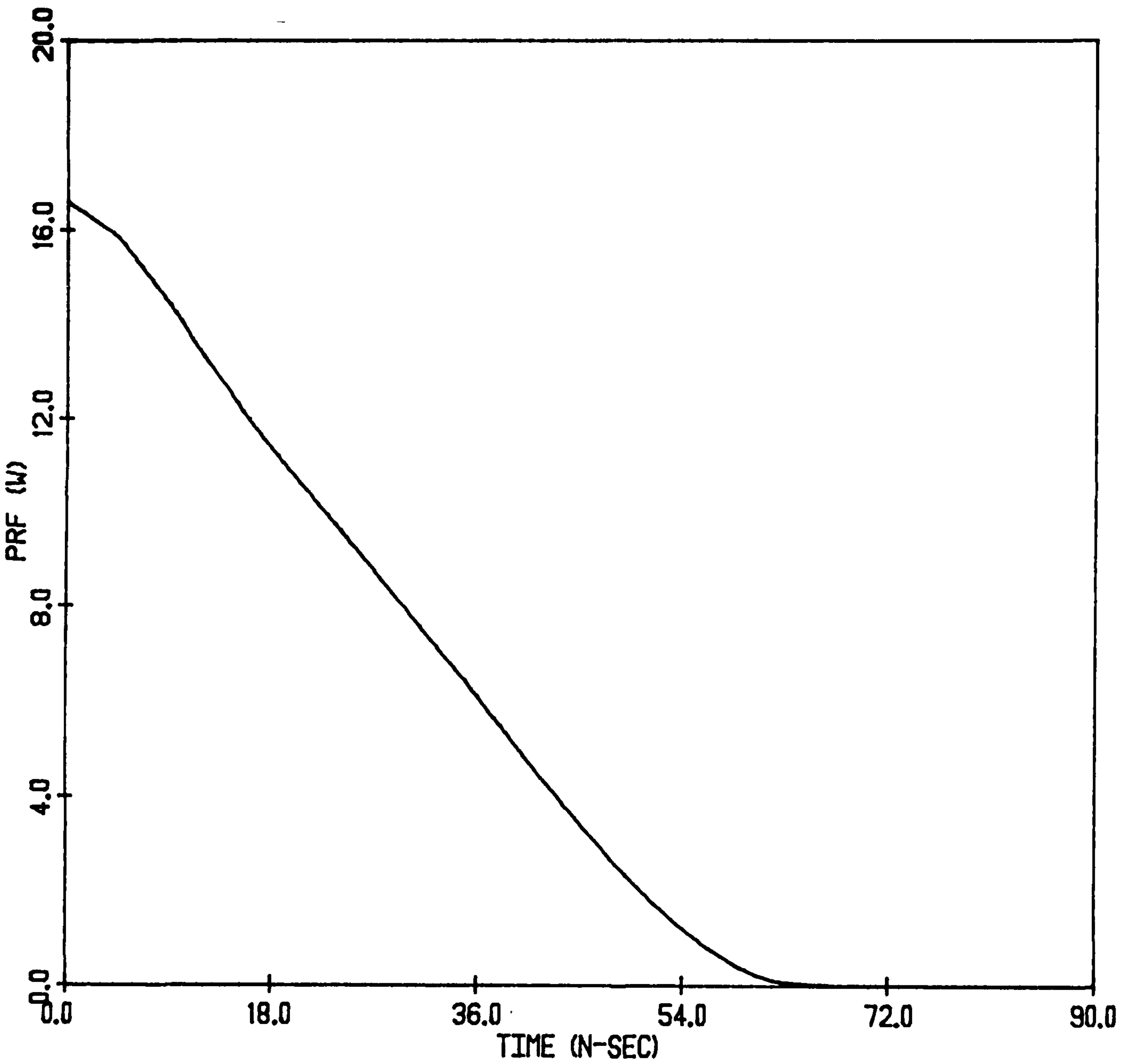

20.0
16.0
12.0
8.0
4.0
0.0
PRF (W)
0.0
18.0
36.0
54.0
72.0
90.0
TIME (N-SEC)

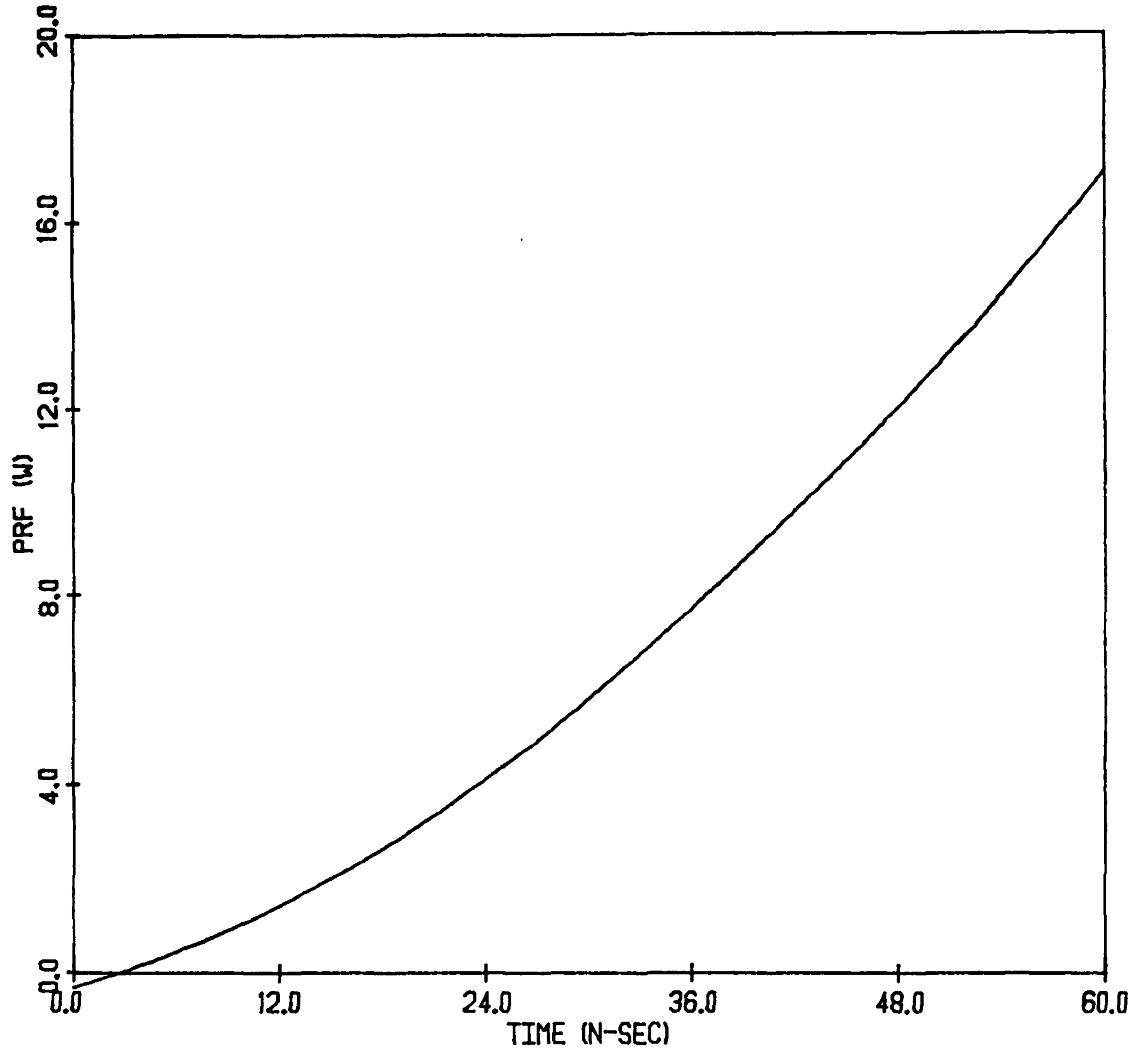
20.0
16.0
12.0
8.0
4.0
0.0
PRF (W)
0.0
12.0
24.0
36.0
48.0
60.0
TIME (N-SEC)

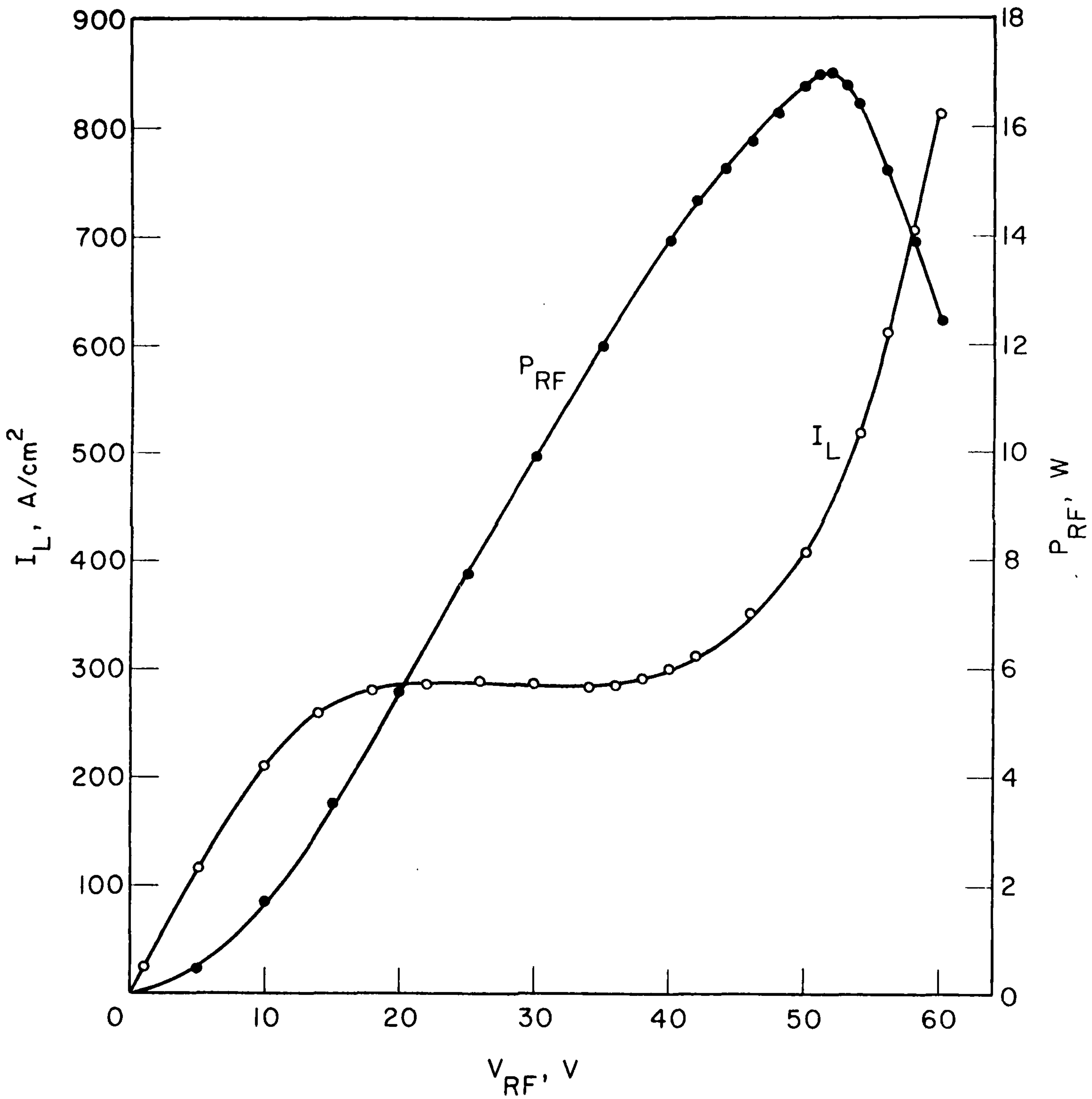

I_L, A/cm^2
P_{RF}, W
V_{RF}, V
P_{RF}
I_L
900
800
700
600
500
400
300
200
100
0
10
20
30
40
50
60
18
16
14
12
10
8
6
4
2

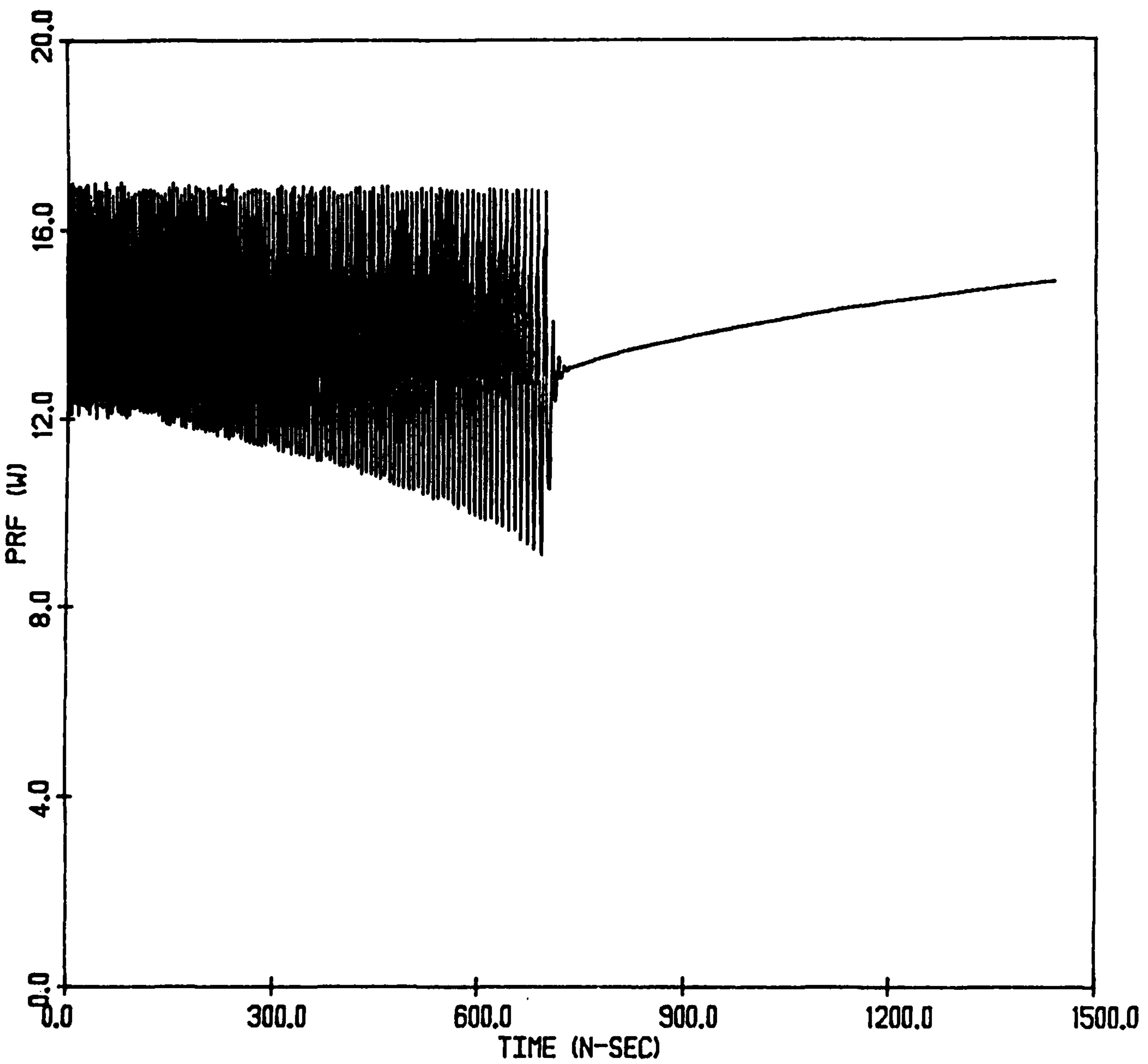

20.0
16.0
12.0
8.0
4.0
0.0
PRF (W)
0.0
300.0
600.0
900.0
1200.0
1500.0
TIME (N-SEC)

END

FILMED

DTIC